MODELLING THE LOW LEVEL RF RESPONSE ON THE BEAM DURING CRAB CAVITY QUENCH

R. Apsimon*, G. Burt, A. Dexter, Lancaster University, Bailrigg, UK
P. Baudrenghien, K. Ness Sjobak, CERN, Geneva, Switzerland
R. Appleby, University of Manchester, Manchester, UK

Abstract

The High Luminosity Upgrade for the LHC (HL-LHC) relies on crab cavities to compensate for the luminosity reduction due to the crossing angle of the colliding bunches at the interaction points. In this paper we present the simulation studies of cavity quenches and the impact on the beam. The cavity voltage and phase during the quench is determined from a simulation in Matlab and used to determine the impact on the beam from tracking simulations in SixTrack. The results of this study are important for determining the required machine protection and interlock systems for HL-LHC.

INTRODUCTION

The High Luminosity Upgrade for the LHC (HL-LHC) uses superconducting RF (SRF) technology for its accelerating and crabbing cavities. During a quench, several physical phenomena occur which affects the behavior of the RF cavity. Before we discuss these phenomena, we remind the reader that the intrinsic quality factor (Q_0) of a cavity is given as

$$Q_0 = \frac{\omega}{\delta\omega} = \frac{\omega U_{\text{stored}}}{P_c}, \tag{1}$$

where ω is the resonant angular frequency of the cavity, $\delta\omega$ is the bandwidth, U_{stored} is the energy stored in the cavity and P_c is the power dissipated in the cavity. As the cavity quenches, the resistive losses in the cavity increase and Q_0 drops. The loaded Q-factor, Q_L, takes into account all power flow out of the cavity, rather than just resistive losses. It is given as $\frac{1}{Q_L} = \frac{1}{Q_0} + \frac{1}{Q_{\text{ext}}}$, where Q_{ext} is the external Q-factor. When $Q_0 \gg Q_{\text{ext}}$, $Q_L \approx Q_{\text{ext}}$, therefore the loaded Q-factor does not change significantly until sometime after the start of the quench. It is assumed that during a quench, Q_0 drops exponentially from its superconducting value (SC) to its normal conducting value (NC) with a transition time τ_{trans}. For the simulations described in the next section, τ_{trans} is assumed to be ~10 µs, based on the assumption that the quench propagates over the cavity surface at the speed of sound in the material; which is approximately 5000 m/s. Table 1 shows the important parameters relating to the HL-LHC crab cavities; values with an asterisk denote values which are assumed or estimated [1].

The power flow into the crab cavity required from a klystron to maintain a transverse voltage, V_{cav}, is given as

$$P_{in} = \frac{V_{\text{cav}}^2}{2\left(\frac{R}{Q}\right)_\perp Q_L}, \tag{2}$$

* r.apsimon@lancaster.ac.uk

Table 1: Nominal Crab Cavity Parameters for HL-LHC [1]

Parameter	Value
Transverse Voltage [MV]	3
Transverse R/Q [Ω]	400
Q_0 [SC/NC]	$10^9/10^3$
Q_{ext}	5×10^5
τ [µs]	10*
Maximum Klystron power [kW]	40 (CW) / 80 (peak)
Resonant frequency [MHz]	400

where $\left(\frac{R}{Q}\right)_\perp$ is the transverse R/Q. Using the parameters in Table 1, the required power to maintain a transverse voltage of 3 MV in the absence of beam loading is 22.5 kW. Assuming the parameters in Table 1, Fig. 1 shows the magnitude of the transverse voltage vs. time in the cavity due to a quench at $t = 0$; all other factors such as detuning, LLRF and beam loading are neglected. It can be seen that the cavity voltage begins to drop ~50 µs after the start of the quench. The cavity voltage then drops rapidly over the next ~50 µs. This is because Q_L does not change significantly until $Q_0 \lesssim Q_{\text{ext}}$.

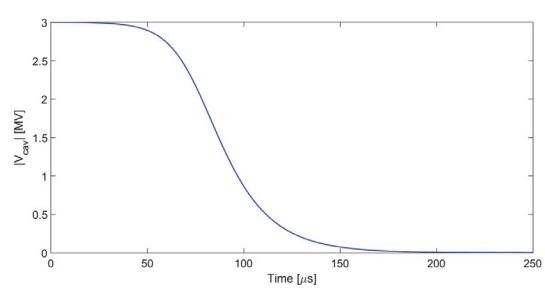

Figure 1: Magnitude of transverse voltage vs. time during a quench, neglecting all other effects.

COMPUTATIONAL MODEL

RF cavities invariably have $Q_L \gg 1$, hence $\delta\omega \ll \omega$. Therefore changes to the fields in the cavity occur over many RF cycles; even during a quench. A simple model of the field in an RF cavity can be described by a second order differential equation describing a driven, damped harmonic oscillator. However as we assume that the amplitude and phase of the cavity voltage cannot vary rapidly, it is more efficient to model the RF envelope with the first order differential equation given in Eq. (3). This envelope equation avoids the need to evaluate the cavity voltage many times

Copyright © 2017 CC-BY-3.0 and by the respective authors

per RF cycle; drastically reducing the required computing power.

$$\frac{\dot{\mathbf{V}}_{\text{cav}}}{\omega_0} + \left(\frac{\omega_0^2 + \omega^2}{4Q_L\omega^2} + i\frac{\omega_0^2 - \omega^2}{2\omega\omega_0}\right)\mathbf{V}_{\text{cav}} = \frac{i\dot{F}_{\text{in}} + \omega F_{\text{in}}}{Q_{\text{ext}}\omega} \quad (3)$$

Here $\mathbf{V}_{\text{cav}}$ is the cavity voltage, expressed as a complex number and F_{in} is a driving term due to the klystron power, given as

$$\mathbf{F}_{in} = \sqrt{2\left(\frac{R}{Q}\right)_{\perp} Q_L \mathbf{P}_{\text{in}}}\,. \quad (4)$$

By inspection, Eq. (3), show that F_{in} and $\dot{F}_{\text{in}}$ are dependent on the LLRF system, ω on the detuning mechanisms. We can model beam loading as an instantaneous change in the amplitude and phase of the cavity voltage when a particle bunch passes through.

Detuning mechanisms

Due to the narrow bandwidth of SRF cavities, they are highly sensitive to detuning mechanisms. For HL-LHC, the crab cavities have a bandwidth of 800 Hz. The dominant detuning mechanisms have been modeled in the simulation.

Lorentz detuning: δf_L The field in the cavity applies a Lorentz force to the surface of the cavity, changing the resonant frequency. This detuning mechanism results in Eq. (3) becoming nonlinear because the coefficients of the equation now implicitly depend on the voltage in the cavity at a given moment in time. For Lorentz detuning, the frequency shifts as

$$\delta f_L = -K_L\left(|\mathbf{V}_{\text{cav}}|^2 + |\mathbf{V}_{\text{nominal}}|^2\right) \quad (5)$$

Resistive detuning: δf_R If we solve the equation of motion for the cavity voltage, we obtain a frequency shift due to the change in Q_L given as

$$\delta f_R = f_0\left(\sqrt{1 - \frac{1}{4Q_L}} - 1\right)\,. \quad (6)$$

Microphonics: δf_m In SRF, mechanical vibrations result in a periodically varying frequency shift, typically of the order of a 100-1000 Hz. This is described as a sinusoidally varying term in the simulations.

Pressure detuning: δf_p SRF structures are cooled in liquid Helium (LHe). During a quench, the cavity surface becomes resistive and power is lost through heat. This heat then boils the surrounding helium, resulting in an increase in pressure on the cavity surface. If the LHe temperature is less than 2.17°K, the helium is superfluid and the pressure detuning is significantly less than for normal fluid helium. In simulation the frequency shift from pressure detuning is modeled as

$$\delta f_p = \frac{K_p}{2}\left(1 + \tanh\left(\frac{t - t_{\text{quench}}}{\tau_p}\right)\right)\,. \quad (7)$$

Lorentz and pressure detuning, like microphonics, are mechanical effects and will excite oscillations. To determine how the frequency shift varies with time, we take the total detuning to be

$$\delta f_{\text{tot}} = \delta f_R + \delta f_{\text{mech}}\,, \quad (8)$$

where δf_{mech} is the solution of the driven harmonic oscillator given in Eq. (9) [2]:

$$\ddot{\delta f}_{\text{mech}} + \omega_m^2 \delta f_{\text{mech}} = \delta f_L + \delta f_m + \delta f_p \quad (9)$$

We have neglected damping in this model.

Low-Level RF system

Lorentz detuning occurs over many RF cycles and pressure detuning can be treated as a transient, Eq. (3) can be considered almost linear over short timescales. Thus a PI-controller is near optimal for controlling the amplitude and phase of the RF cavity voltage. The PI controller response is given as

$$\delta\mathbf{F}_{in} = c_p\left(\mathbf{V}_{\text{cav}} - \mathbf{V}_0\right) + c_i\sum_t\left(\mathbf{V}_{\text{cav}} - \mathbf{V}_0\right)\,, \quad (10)$$

where c_p and c_i are the coefficients for the proportional and integral controllers.

RESULTS

The simulation code was used to recreate the observed behavior of the KEKB crab cavities during a quench [3], then used to model a quench of the HL-LHC crab cavities.

KEKB observed up to 50° phase shifts within 50 µs, with approximately 75% of the nominal field in the cavity. For HL-LHC, catastrophic beam losses would occur within 3 turns of the ring; preventing any possible beam dump and resulting in substantial damage. Table 2 highlights the differences between the KEKB and HL-LHC crab cavities (CCs).

Table 2: Comparison Between the KEKB and HL-LHC CCs

Parameter	KEKB	HL-LHC
Beam energy [GeV]	8	7000
Transverse R/Q [Ω]	50	400
Q_0	10^9	10^9
Q_{ext}	1×10^5	5×10^5
Operating temperature [K]	2	4

For machine protection system, KEKB turned off the RF power as soon as a quench is detected, before the beam is dumped; whereas HL-LHC will keep the RF power on until after the beam is dumped to minimize losses.

Figures 2 and 3 show the phase and amplitude of the transverse voltage for a KEKB-like and HL-LHC-like cavity during a quench, respectively.

For the KEKB-like crab cavity, the magnitude (Fig. 2, top) drops earlier and less smoothly than for the HL-LHC crab cavity (Fig. 3, top) due to the RF being switched off. The

Copyright © 2017 CC-BY-3.0 and by the respective authors

ISBN 978-3-95450-182-3

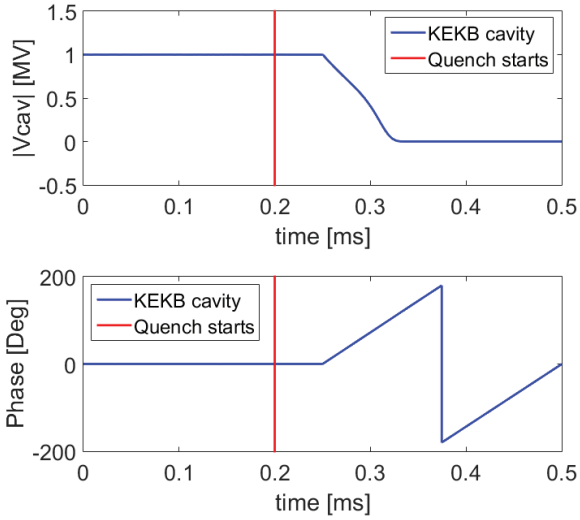

Figure 2: Magnitude (top) and phase (bottom) of the voltage for a KEKB-like crab cavity during a quench.

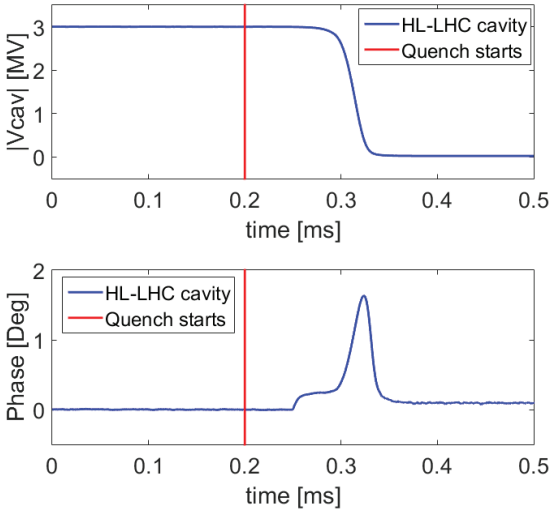

Figure 3: Magnitude (top) and phase (bottom) of the voltage for a HL-LHC-like crab cavity during a quench.

KEKB-like cavity is cooled in non-superfluid Helium and therefore experiences significant pressure detuning during a quench, which results in a large and sustained phase shift (Fig. 2, bottom). By contrast, the HL-LHC crab cavity experiences significantly less pressure detuning, but greater Lorentz detuning due to the higher cavity voltage.

Figure 4 shows the results from tracking simulation using SixTrack [4, 5] for the HL-LHC beam at 7 TeV during a crab cavity quench. Here the voltage and phase of the upstream cavity closest to IP1 in beam 1 was loaded from the cavity model, and the effect on the beam evaluated. Each bunch was represented by 40,000 particles, sampled from a double-Gaussian distribution [6]. These were tracked for 100 turns with constant voltage and phase in order to clean most high-

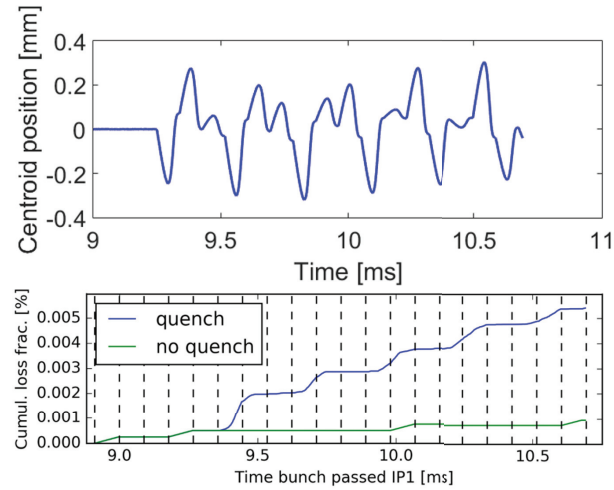

Figure 4: SixTrack simulation of a the mean beam position at the cavity (top) and the beam losses during a quench (bottom) of a HL-LHC-like crab cavity; vertical lines indicate turns.

amplitude particles, and then 20 turns more after the onset of the failure. Two cases were ran, one where the control loop was operating normally and one with a quench. The top plot shows the shift in beam centroid position during a quench and the bottom plot shows the fractional beam loss vs. time during the quench. This shows that the losses due to the quench are small, in the order of 0.005% of the full beam, which is in line with what has been found for similar scenarios [6, 7]. Furthermore, the beam centroid movement remains small compared to the beam size at the cavity ($\sigma \approx 1$ mm).

Additional studies with sector maps, produced by MADX [8], were also undertaken and showed that for a KEKB-like machine, a quench of one of the crab cavities results in total beam loss due to the low beam rigidity even with the RF kept on. Hence turning off the RF system prevents potential damage to the klystrons. For the HL-LHC crab cavities, the centroid position move very little, but with the RF switched off this motion increases by a factor of 5-10, risking additional beam loss.

CONCLUSION

In this paper, we present simulation studies of crab cavity quenches. We used the simulation to model a KEKB-like crab cavity in order to benchmark against measured data and the simulations successful reproduced the observed rapid phase shift before the cavity voltage drops. Using the simulation to model the HL-LHC crab cavities, we conclude that the maximum phase shift during a quench would be 1-2° before recovering to within 0.1° of nominal as the RF system will be left on during a quench.

ACKNOWLEDGMENT

The authors would like to thank Rama Calaga and Alejandro Castilla Loeza for their help and advice for the content of this paper.

Copyright © 2017 CC-BY-3.0 and by the respective authors

REFERENCES

[1] HL-LHC technical design report, to be published

[2] K. Sjobak *et al.*, "Time Scale of Crab Cavity Failures Relevant for High Luminosity LHC", in *Proc. 6th Int. Particle Accelerator Conf. (IPAC'16)*, Busan, Korea, May 2016, paper THPOY043, pp. 4196–4199.

[3] K. Nakanishi *et al.*, "Beam Behaviour due to Crab Cavity Breakdown", in *Proc. 1st Int. Particle Accelerator Conf. (IPAC'10)*, Kyoto, Japan, May 2010, paper WEPEC022, pp. 2938–2940.

[4] G. Robert-Demolaize, R. Assmann, S. Redaelli, and F. Schmidt, "A new version of SixTrack with collimation and aperture interface", in *Proc. of PAC'05*, paper FPAT081.

[5] K. Sjobak, H. Burkhardt, R. De Maria, A. Mereghetti, and A. Santamaría García, "General functionality for turn-dependent element properties in SixTrack", in *Proc. 5th Int. Particle Accelerator Conf. (IPAC'15)*, Richmond, VA, USA, May 2015, paper MOPJE069, pp. 468–471.

[6] A. Santamaría García *et al.*, "Machine protection from fast crab cavity failures in the High Luminosity LHC", in *Proc. 6th Int. Particle Accelerator Conf. (IPAC'16)*, Busan, Korea, May 2016, paper TUPMW025, pp. 1485–1488.

[7] K. Sjobak and A. Santamaría García, "Crab cavity failure modes and mitigation", presentation at the 6th HL-LHC collaboration meeting, Paris, France, November 2016, `https://indico.cern.ch/event/549979/contributions/2295073/attachments/1371504/2080340/2016-11-14_HLLHC_Paris-CrabFailures-Kyrre.pdf`

[8] "Methodical Accelerator Design", `http://madx.web.cern.ch/madx/`

Copyright © 2017 CC-BY-3.0 and by the respective authors

ISBN 978-3-95450-182-3